High Contrast Imaging with Gaussian Aperture Pupil Masks

John H. Debes & Jian Ge

Pennsylvania State University, 525 Davey Lab, University Park, USA

ABSTRACT

Gaussian aperture pupil masks (GAPMs) can in theory achieve the contrast requisite for directly imaging an extrasolar planet around a nearby solar type star. We outline the process of designing, fabricating, and testing a GAPM for use on current telescopes and specifically the Penn State near-IR Imager and Spectrograph (PIRIS) at the Mt. Wilson 100″ telescope. We find that the initial prototype observations are quite successful, achieving a contrast similar to a traditional Lyot coronagraph without blocking any light from a central object and useful for finding faint companions to nearby young solar analogues. In the lab we can reproduce the expected PSF reasonably well and with a single aperture design which achieves $\sim 4 \times\ 10^{-5}$ contrast at $10\lambda/D$. We find that small inaccuracies in the mask fabrication process and insufficient correction of the atmosphere contribute the most degradation to contrast at these levels.

Subject headings: high contrast imaging, apodization, extrasolar planets, coronagraphy

1. Introduction

The search to directly image an extrasolar planet around a nearby solar type star requires contrast levels of $\sim 10^{-10}$ a few λ/D from the central star, where λ is the wavelength of light observed and D is the diameter of the observing telescope's primary mirror. Scattered light in a telescope and the diffraction pattern of the telescope's aperture limit the contrast possible for direct detection of faint companions (Brown & Burrows 1990). The circular aperture of telescopes creates a sub-optimal diffraction pattern, the so-called Airy Pattern which is azimuthally symmetric. In addition, the intensity in the diffraction pattern of the circular aperture declines as $(\theta/\theta_o)^{-3}$ where $\theta_o = \lambda/D$. Currently the best way to diminish the Airy pattern is to use a coronagraph by using the combination of a stop in the focal plane that rejects a majority of the central bright object's light and a Lyot stop in the pupil plane to reject residual light diffracted to the edge (Lyot 1939; Malbet 1996; Sivaramakrishnan

2001). Several recent ideas explore the use of alternative "apodized" apertures for high contrast imaging in the optical or near-infrared (Nisenson & Papaliolios 2001; Spergel 2001; Ge 2002; Kuchner & Spergel 2003a). These designs revisit concepts first experimented with in the field of optics (Jacquinot & Roizen-Dossier 1964). Other designs, such as the band limited mask or notch-filter mask, seek to null the light from a central star by varying either the amplitude of the central star's light in the focal plane (Kuchner & Traub 2002; Kuchner & Spergel 2003b; Debes 2004).

All of these designs in theory can reach the contrast ratio necessary for imaging a planetary companion, however most of these concepts are just starting to be tested in the lab or on a real telescope where other concerns arise. Each design also has its own set of drawbacks. Pupils or image plane masks that require transmissive functions require precision to very high levels (10^{-10}) and are suceptible to degradation in a space environment (Kuchner & Spergel 2003a). Designs that use binary masks have less restrictive tolerances but must be fabricated precisely. The specific advantages of each idea cannot be determined until they are actually built and tested in such a way as to simulate real observing conditions.

Apodization through binary shaped apertures that have either completely transmissive or completely opaque openings represent one promising class of techniques. An intuitive description of how the choice of a shaped aperture affects the resulting PSF is in order. The entrance aperture can be described as a contour $y\prime = \pm(1/2)C(x\prime)$, where $|x\prime| < x\prime_M$ the maximum horizontal extent of the aperture. An example of a familiar contour for an entrance aperture is $C(x\prime) = \sqrt{x\prime_M - 4x\prime^2}$, the equation for a circular aperture. The resulting point spread function (PSF) as predicted by scalar Fraunhoffer diffraction theory is given by the 2-D Fourier transform of the aperture:

$$\mathcal{A}(\xi\prime, \eta\prime) = \int_{-x\prime_M}^{x\prime_M} \int_{-\frac{1}{2}C(x\prime)}^{\frac{1}{2}C(x\prime)} \exp(2\pi k i \xi\prime x\prime) \exp(2\pi k i \eta\prime y\prime) \mathrm{d}x\prime \mathrm{d}y\prime \tag{1}$$

where $k = 2x\prime_M/\lambda$ and we follow the notation of Jacquinot & Roizen-Dossier (1964). We then transform this equation into the reduced coordinates $x = x\prime/2x\prime_M, y = y\prime/2x\prime_M, \xi = 2\xi\prime x\prime_M/\lambda$, and $\eta = 2\eta\prime x\prime_M/\lambda$. The equation then becomes:

$$\mathcal{A}(\xi, \eta) = \int_{-\frac{1}{2}}^{\frac{1}{2}} \int_{-\frac{1}{2}C(x)}^{\frac{1}{2}C(x)} \exp(2\pi i \xi x) \exp(2\pi i \eta y) \mathrm{d}x \mathrm{d}y. \tag{2}$$

This two dimensional problem can be simplified to a one dimensional Fourier transform provided the PSF is restricted to a particular $\eta = \eta_o$:

$$\mathcal{A}(\xi, \eta_o) = \int_{-\frac{1}{2}}^{\frac{1}{2}} \frac{\sin(\pi \eta_o C(x))}{\pi \eta_o} \exp(2\pi i \xi x) \mathrm{d}x \tag{3}$$

By sampling η to the desired precision one can build up a 2-D PSF by performing a 1-D Fast Fourier Transform (FFT) (Lieber 2003). In this way the PSF can be determined with more accuracy and less time than with traditional 2-D FFTs. There exists the special case of the diffraction pattern along the $\eta = 0$ axis, which even more greatly simplifies the expression by becoming a simple Fourier Transform of $C(x)$:

$$\mathcal{A}(\xi, 0) = \int_{-\frac{1}{2}}^{\frac{1}{2}} C(x) \exp(2\pi i \xi x) \mathrm{d}x \tag{4}$$

Binary shaped apertures where $C(x)$ is described as a truncated Gaussian function represent a promising design for high contrast imaging and was suggested for extrasolar planet searches by Spergel (2001). However, the idea has potential uses on ground based telescopes as well for more modest goals, such as high contrast imaging surveys that cannot afford to take the overhead of aligning coronagraphic masks or who observe multiple targets in one field of view (Ge 2002). In this case the gaussian contour is

$$C(x) = a \left\{ \exp\left[-(2\alpha x)^2 \right] - \exp\left(-\alpha^2\right) \right\}. \tag{5}$$

Since the Fourier transform of a gaussian function is another gaussian, the amplitude of the diffraction pattern $A(\xi, \eta)$ along the ξ axis decreases like $\mathrm{e}^{-\xi^2}$, which we denote the high contrast axis. The intensity distribution in the imaging plane is given by $|AA^\star|$. The ratio $z = I(\xi, \eta)/I(0, 0)$ gives the contrast relative to the peak intensity of the diffraction pattern. The variables a and α are free parameters that can be used to optimize the aperture for depth of contrast, the angle from the central object at which high contrast starts, and the azimuthal area of high contrast. It should be noted that based on this definition, changing α subtly changes the height of the contour since the maximum height of the contour is $\propto 1 - \exp(-\alpha^2)$. However, in terms of the range of α that we test and are interested in ($\alpha = 2 - 4$) for realistic observations, this is a negligible effect on the order of a few percent.

The final peak intensity $I(0, 0)$ measured on a detector is proportional to the total area of the aperture squared. In the reduced coordinates that we use, a square, fully transmissive aperture gives the maximum intensity, which we normalize to one (Jacquinot & Roizen-Dossier 1964). In this normalization, a circular aperture gives rise to a maximum intensity of $\pi^2/16$. Determining the peak intensity for a GAPM then requires summing the total area of the given aperture and squaring it:

$$I(0, 0) = \left| \int_{-\frac{1}{2}}^{\frac{1}{2}} C(x) \mathrm{d}x \right|^2. \tag{6}$$

Solving this for Equation 5, gives $I(0, 0) = (a\sqrt{\pi}\mathrm{erf}(1/2)/(2\alpha) - a\exp(-\alpha^2))^2$. We can compare this to a circular aperture. For an $\alpha = 2.7, a = 1$ GAPM, this corresponds to

a peak intensity 3% of a full circular aperture. A Lyot stop that undersizes the circular aperture by 1/2 gives a peak 6.25% of the original. Light gathering power is proportional to the area, and so for the same examples, the Lyot coronagraph would have 25% throughput and the GAPM 17%.

By substituting Equation 5 into Equation 3, the PSF can be determined. Figure 1 shows the resulting PSF for an aperture with $a = .6$ and $\alpha = 2.9$, a typical pattern from a Gaussian contour. Since the contour is not azimuthally symmetric neither is the PSF, with a region that has high contrast, which we denote the high contrast region (HCR). High contrast is deepest along the ξ axis.

If one is designing a mask, it would be useful to have several first order estimates of the dependance of a and α on the resulting diffraction pattern. We start with the contrast along the axis of highest contrast and an approximate separation in ξ where high contrast starts. The exact solution of Equation 4 is given by

$$\mathcal{A}(\xi, 0) = \frac{\sqrt{\pi}}{2\alpha} \exp\left[(\pi\xi/2\alpha)^2\right] \star \mathrm{sinc}(\xi) - 2\exp(-\alpha^2)\mathrm{sinc}(\xi), \tag{7}$$

where $\mathrm{sinc}(\xi) = \sin(\pi\xi)/\pi\xi$. This is difficult to manipulate analytically, but can be approximated to first order by

$$A(\xi, 0) = \frac{\sqrt{\pi}}{2\alpha} \exp[-(\pi\xi/2\alpha)^2] - \exp[-\alpha^2]\mathrm{sinc}(\xi), \tag{8}$$

which ignores the truncation of the exponential part of the function.

The width of the PSF core can then be estimated by determining the location of the first zero (ξ_{fz}) in Equation 8. After some manipulation one finds that

$$\xi_{fz}^2 = \frac{4\alpha^2}{\pi^2}\left[\alpha^2 - \ln|\mathrm{sinc}(\xi_{fz})| + \ln|\frac{\sqrt{\pi}}{2\alpha}|\right]. \tag{9}$$

One can solve this equation exactly through a simple recursion algorithm. However, noting that $\ln|\mathrm{sinc}(\xi)| \sim 3$ over the range of ξ we are interested in ($\xi = 3 - 10$), that $\ln|\frac{\sqrt{\pi}}{2\alpha}| \sim -1$ over the range of interesting α values ($\alpha = 2 - 4$), and assuming $\alpha^2 \gg 2$,we find that Equation 9 is well approximated by:

$$\xi_{fz} = \frac{2\alpha^2}{\pi}\left(1 + \frac{1}{\alpha^2}\right). \tag{10}$$

The approximate contrast one can expect to achieve is then found by substituting ξ_{fz} into Equation 8 and squaring the result. Finally, one can estimate the angular coverage

of the HCR by noticing the HCR is governed by the tail of the Gaussian function, which transitions over at the contour's change of curvature. By solving for the maximum angle where the change occurs on the aperture, the resulting angle of high contrast in the imaging plane is given by

$$\cot\theta = \sqrt{\frac{2}{e}}a\alpha. \tag{11}$$

By placing a mask into the pupil plane with a Gaussian aperture, one can transform a traditional circular aperture telescope into one with a diffraction pattern better suited for high contrast imaging. Using a mask represents a quick, efficient, and economical way to test this emerging imaging method to determine its advantages and tradeoffs and compare them to the performance of other existing techniques. More subtle phenomena that limit contrast can also be studied and removed with a well-known system whose ideal performance and performance under non-ideal conditions can be easily modeled. Scattered light from microroughness or polarization effects can be more reliably studied and verified experimentally rather than with completely theoretical treatments.

We have endeavored to begin anwering the question of which design ultimately will be useful in the search for extrasolar planets, or which will be most useful for other areas of astronomy where less stringent tolerances are present. To that end we have designed, fabricated, and tested several GAPM designs for use with the Penn State near-IR Imager and Spectrograph (PIRIS)(Ge 2003). In Section 2 we explore what the best design for a telescope would be. In Section 3 we briefly discuss the process of fabrication of the GAPMs, while in 4 we discuss the various tests we performed in the lab and on the ground at the Mt. Wilson 100″ telescope. Finally in Section 5 we discuss what role GAPMs have for future high contrast imaging.

2. Designing a GAPM for current telescopes

The idealized design of a single gaussian aperture in practice cannot be used on current telescopes due to their circular secondary obstructions and the presence of the support structure. These two additions serve to modify the resulting diffraction pattern and destroy the advantages of the single aperture. Therefore, a new design that avoids or minimizes their effect is necessary to retain high contrast. There are two possible solutions: multiple apertures that avoid the structure completely, or a way of blocking the structure without changing the diffraction pattern in the imaging plane, such as with another gaussian curve.

2.1. Multiple Apertures

By taking a contour over a sub-aperture of width hD where D is the diameter of the telescope pupil, one reproduces a similar diffraction pattern as obtained from the contour described in Equation 5 with the exception that ξ and η must be rescaled by dividing by h. Placing multiple subapertures on the pupil as the convolution of the base subaperture with a sum of N δ-functions in the desired positions of the subapertures. The Fourier transform of that convolution becomes:

$$\mathcal{A}'(\xi,\eta) = \mathcal{A}(\xi,\eta)\sum_{k=1}^{N}\exp(2\pi i x_k\xi)\exp(2\pi i y_k\eta). \tag{12}$$

As mentioned in Spergel (2001) and Kasdin (2003), one can also have multiple apertures with asymmetric sides as long as they are reflected about the y-axis. In this case the contour can be described on the full pupil in the original reduced coordinates of Equation 1 as

$$\begin{aligned} C_1\left(\frac{x}{h}\right) &= hC\left(\frac{x}{h}\right) + 2y_o \\ C_2\left(\frac{x}{h}\right) &= -\frac{hb}{a}C\left(\frac{x}{h}\right) + 2y_o \end{aligned} \tag{13}$$

where y_o is a constant vertical offset from the y-axis and a is not equal to b. The resulting diffraction pattern is the superposition of the PSF from the two contours. Either approach can yield a grouping of apertures that completely avoids the support structures and maximizes the possible throughput. The potential tradeoff is a widening of the PSF core, as well as a new peak that is multiplied by a factor of Nh^4.

2.2. Minimizing Support Structure

Another option for avoiding the secondary of a telescope is to create an opaque secondary gaussian curve that blocks the circular secondary mirror. The result in the focal plane would be the superposition of PSFs, which follows naturally from the Babinet principle. One way of implementing this design is to have a contour similar to Equation 5 but with a second contour with a height b where $b < a$:

$$\begin{aligned} C_1(x) &= aC(x) \\ C_2(x) &= -bC(x). \end{aligned} \tag{14}$$

The resulting PSF retains the higher resolution of the telescope, though angular coverage may be less than what could be achieved with multiple apertures.

In this case it is important to estimate the effect of not avoiding the support structure. The level of contamination by the support vanes for the secondary mirror can be estimated by deriving the diffraction pattern for a slit with the same proportions of the vanes and using Babinet's principle. A vane of width w along the x-axis and length l in the y-axis has an amplitude of

$$\mathcal{A}_s(\xi,\eta) = wl\mathrm{sinc}(\xi w)\mathrm{sinc}(\eta l). \tag{15}$$

The vane will be brightest along the ξ axis. Ideally, support vanes should be rotated 45° with respect to the HCR, so that the diffraction spikes can be masked by the lower contrast regions of the PSF. $\mathcal{A}_s$ can be compared to $\mathcal{A}(0)$. If $\mathcal{A}_s \ll \mathcal{A}(0)$, and the secondary is not so large that the loss in throughput is great, this method may be preferable. As an example we look at spider vanes that have a width of $\sim 10^{-3}D$, which corresponds to a contrast of 10^{-8} at a distance of $5\lambda/D$ assuming that the two vanes are oriented 45° to the axis of interest. Clearly this places a fundamental limit on the width of any support structure (or gaps in a multi-mirror design) for an extrasolar planet search. Taking the limiting contrast to be 10^{-10} at $5\lambda/D$, the size limit is $10^{-4}D$.

2.3. Final Design of the Prototype

We designed a mask to be used at the Mt. Wilson 100″ telescope for preliminary observations, as well as a single aperture design for testing in the lab. The diameter of the secondary at Mt. Wilson is ∼30% the diameter of the primary and the width of the spider vanes are ∼.25% of the diameter. We decided to completely avoid the support structure for the initial prototype to lower the risk of the PSF being contaminated by misalignments of the pupil mask. For a final design we decided to try a variation of what was proposed by Spergel (2001), using a contour based on Equation 13 by placing 3 sub-apertures in each quadrant of the mask to maximize throughput to about 16%. Table 1 shows the parameters that we used for the two masks as well as the positioning of the apertures for the Mt. Wilson design. Figure 2 shows what the final design looked like. Figure 3 shows a comparison between a J band image taken with the mask and a theoretical PSF modeled by taking digital images of the apertures at high magnification and taking a 2D FFT with IDL. Since the spatial scale of the PSF determined in Equation 2 is scalable with wavelength, one can build a multi-wavelength PSF by adding the scaled PSF in wavelength bins together and multiplying by the transmission of the particular filter used.

3. Fabricating a GAPM

Once a design was chosen the masks were fabricated. We chose to fabricate the Mt. Wilson and lab designs with Photo-Chemical Machining (PCM). This technique has been used to produce masks to block thermal radiation from telescope structures for near-IR observing and for creating Lyot stops (McCarthy 2001).

The process of PCM, also called Photo-Etching or Photo-Chemical Milling, involves using a thin metal sheet that is coated with a light sensitive polymer. A UV photo imaging tool is used to imprint the desired design on the sheet. It is then developed much like film and chemically etched by an aqueous solution of ferric chloride ($FeCl_3$).

Several masks are present in the PIRIS camera mainly for the traditional Lyot coronagraphic modes. They were fabricated by Newcut, Inc. (Newark, NJ). For the GAPMs we submitted CAD designs based on the simulations performed to Newcut and they fabricated the masks. A sheet of 25-50 masks with a diameter of ~ 4 mm were fabricated at very low cost within a few weeks. When they were delivered they were photographed on an optical telescope with 5x and 50x magnification.

This technique can provide the basic shape we need, but has difficulty preserving the exact shape of the design in the smallest regions. The edges of the gaussians on the mask were truncated well before they mathmatically would be. Variations on the order of 10 μm are also observed in the masks. Both of these imperfections can degrade contrast, which is discussed further in Section 4. These imperfections are likely caused by the photo printing as well as the chemical etching. For instance, the corner truncation and width variation can be caused by underexposure of the light sensitive polymer. The rugged edge can be caused by non-uniform chemical etching. Since the etching is isotropic, changes in the physical and chemical conditions of the etchant can cause local irregularities.

4. Testing the Prototype

4.1. First Light and Lab tests

We placed the Mt. Wilson design on the Penn State Near-IR Imager and Spectrograph (PIRIS) and ran tests both in the lab and on the 100″ Mt. Wilson telescope. We used the prototype as part of a survey for faint companions around nearby solar type stars (Chakraborty et al. 2002; Debes et al. 2002).

Further details are outlined in Debes et al. (2002). We used the prototype GAPM to

study two stars, ϵ Eridani and μ Her A. The mask allowed confirmation of a common proper motion companion to μ Her A and placed limits on any possible companions around ϵ Eridani down to the level of a $38M_{jup}$ brown dwarf. This corresponds to a performance an order of magnitude better than adaptive optics alone and 2 times worse than our Lyot coronagraph performance without blocking the central star's light (Debes et al. 2002).

Lab testing was also performed in the J and H bands on the Mt. Wilson design. The setup involved taking an incandescent lamp and simulating a point source to sample the PSF generated by the different masks. An optical fiber took light from an incandescent lamp where it passed through a micro objective and a pinhole. The light then was collimated by a collimator achromat. After the collimator it was focused onto the slit wheel aperture by an image achromat. The image achromat also forms an exit pupil, $\sim$1.9 m away from the focal plane, mimicking the Mt. Wilson $100''$ exit pupil. On the slit wheel we placed our focal plane coronagraphic masks. The light then travels through the camera optics of PIRIS where it is read by the 256×256 PICNIC array.

Figure 4 shows an azimuthally averaged comparison between the data taken at Mt. Wilson, lab tests in the J band, and two theoretical multiwavelength PSFs as a function of λ_o/D, where λ_o represents the central wavelength of the filter used. For the lab and models this corresponds to using a J filter whereas on Mt. Wilson all observations were done in the K band. Azimuthal averaging was performed over $\pm 30^\circ$ from the high contrast axis on both sides. One simulation, called model 1, represents a completely ideal situation where the mask is perfectly created and no wavefront errors exist. The second simulation, model 2, takes the observed shape of the masks under magnification as the apertures and neglects other errors. One can see that the theoretical simulation of the observed shape matches the lab data quite well, off by less than an order of magnitude close to the center. The observed shape errors also degrade the contrast achievable by the idealized design. Finally the effect of the atmosphere is present in the Mt. Wilson data. From our observations, the seeing was $\sim 1''$, giving an $r_o \sim 46$ cm at 2.2 μm . We estimate that our Strehl ratio for most of the observations was lower than expected, $\sim$.1. At this level of correction the halo from the atmosphere severely degrades the contrast to $\sim 10^{-2}$.

From images of the pupil optics of PIRIS, we observed low amounts of light leakage and thermal emission. This slightly degrades contrast, which would explain the slight difference between our models and the observed lab PSF.

The single aperture GAPM was also tested in the J band in the lab. Figure 5 shows the contrast achieved with an azimuthal average over $\pm 20^\circ$ with respect to the high contrast axis. The truncation present in the fabrication also severely degrades the contrast possible with this mask. We find that we can achieve a contrast of $\sim 10^{-5}$ at $10\lambda/D$.

4.2. Modeling the Degradation in Contrast

Figure 2 shows one of the greatest limitations to the current prototype, which is the truncation of the thinnest parts of the mask. This is due to errors in the fabrication process as well as a lack of resolution to reproduce the true contour. We can model this effect by taking images of the apertures and digitizing them into model apertures, which has been shown above to be effective in Figures 3 and 4.

There is also a way to express this analytically, by slightly changing the contour of the aperture:

$$C(x) = a\left\{\exp\left[-(2\alpha x)^2\right] - \exp(2\beta x)\exp\left(-\alpha^2\right)\right\}, \tag{16}$$

where β is a free parameter that can be determined empirically. The effect of this change raises the floor of contrast by increasing the strength of the second term in Equation 16.

Figure 6 shows a comparison between the observed multi-wavelength PSF of our prototype Mt. Wilson design and a model based on Equation 16 both azimuthally averaged over 20° around the high contrast axis. A β=13 matches the observed PSF and the models based on the fabricated apertures quite well.

Another potential problem beside truncation of the edges is the tolerance for accuracy in the mask itself. We can estimate the effect by considering either a square opening or obstruction of side h depending on the kind of error that occurred. This extra square will create its own diffraction pattern that will constructively add to the PSF. Using the same equation as in Equation 15, we can estimate the intensity due to the total number of errors present for a particular distance, $(\sim N_{err}h^2/\pi\xi)^2$, where N_{err} is the total number of errors present. In the case of errors due to the resolution of a fabrication method one can base the estimate on the fact that the number of errors will be $\sim h^{-1}$ where we assume the size of the error is no bigger than the resolution of the machine. This leads to the contrast degrading as h^2. In order to reach a contrast of 10^{-10} at $4\lambda/D$, errors are restricted to $< 10^{-4}D_p$, where D_p is the pupil mask diameter. For a pupil mask with a diameter of 4 mm, this corresponds to a resolution of .4 μm.

4.3. Lessons for AO observers

The lessons that can be gained from the AO observations can be put to use for future work. It is clear that a high order of correction is needed for the full advantage of the GAPM to be utilized. Ideally one would choose an inner working distance (IWD) that is less than the region that is fully corrected (to the level of the residual halo) by the AO system.

This angle, $\theta_c = N_{act}\lambda/2D$, depends on the number of actuators across the diameter of the primary (Sivaramakrishnan 2001). For Mt. Wilson, this area extends out to $8\lambda/D$ so a design with an IWD of closer to $4\lambda/D$ or less would be ideal.

Ground based observations are also limited by the contrast ratio of the uncorrected halo to the core ($z_{\rm halo}$). The FWHM of the halo is approximately the uncorrected seeing, which typically is $> \theta_c$. In that case a good estimate of the best contrast achievable is simply the ratio of the peak intensity of the uncorrected halo to the peak intensity of the corrected image core (Hardy 1998):

$$z_{\rm halo} = \frac{1-S}{1+\left(\frac{D}{r_o}\right)^2}, \tag{17}$$

where S is the Strehl Ratio, r_o is the Fried Parameter of atmospheric turbulence, and D is the diameter of the telescope. Roberts & Neyman (2002) has reported S values of $\sim$.2 for the AEOS telescope in the visible (.55 μm) for an $r_o \sim 12$ cm, giving an approximate contrast of 10^{-3}. In this case, larger telescopes gain an advantage in contrast given the same seeing conditions and ability to attain a certain Strehl ratio. Higher order adaptive optics will need to correct to very high levels (S$\sim$ .9) to successfully achieve a high contrast with a GAPM. However, using a more modest α with a more modest level of high contrast may present a useful alternative to a coronagraph for groundbased searches with AO, for example in relatively dense young clusters or for faint companion searches to white dwarfs.

5. Conclusions

We have performed several simulations, lab tests, and telescope observations with GAPMs in order to better understand the interplay between theory and the reality of observations. GAPMs alone provide an improvement over a simple circular aperture for quick high contrast imaging. They are very sensitive to an accurate reproduction of shape and thus need accuracies that require nanofabrication techniques such as e-beam lithography, similar to what has been used for notch-filter masks (Debes 2004). We have commissioned some precise GAPMs with accuracies on the order of .25 μm which should lead to a more accurate shape reproduction and a minimization of errors. Precisely fabricating these masks can potentially improve performance to the ideal limit for a mask provided it is above the scattered light limit of the telescope, bringing it in line with Lyot coronagraphs of comparable throughput. Demonstration of these masks in conjunction with an adaptive optics system could present a workable example of a quick way to survey for faint companions without needing to incur the overhead cost of precise alignment behind a coronagraphic image mask.

The authors would like to acknowledge D. McCarthy for loaning part of the optics for PIRIS, R. Brown (LPL) for the PICNIC array, C. Ftaclas for coronagraphic masks, and A. Kutyrev for filters. Several important comments from the anonymous referee were particularly useful as well as discussions with D. Spergel and M. Kuchner which were crucial in our understanding of gaussian apertures and band limited masks. We would also like to thank the invaluable help of the the Mt. Wilson staff, L. Engel for design help with the GAPM, Abhijit Charkraborty, and Dan McDavitt for help providing figures.

This work was supported by NASA with grants NAG5-10617, NAG5-11427 by NSF with grants NSF ASTRO-0138235 by Ball Aerospace, Inc. as well as the Penn State Eberly College of Science. J.D acknowledges funding by a NASA GSRP fellowship under grant NGT5-119.

REFERENCES

Brown, R. A. & Burrows, C. J. 1990, Icarus, 87, 484

Chakraborty, A., Ge, J., & Debes, J. H. 2002, AJ, 124, 1127

Debes, J. H., Ge, J., & Chakraborty, A. 2002, ApJ, 572, L165

Debes, J. H. e. a. 2004, ApJ, (in press)

Ge, J. e. a. 2002, in Future Research Direction and Visions for Astronomy. Edited by Dressler, Alan M. Proceedings of the SPIE, Volume 4835, pp. 87-97 (2002)., 87–97

Ge, J. e. a. 2003, in Instrument Design and Performance for Optical/Infrared Ground-based Telescopes. Edited by Iye, Masanori; Moorwood, Alan F. M. Proceedings of the SPIE, Volume 4841, pp. 1503-1514 (2003)., 1503–1514

Hardy, J. W. 1998, Adaptive optics for astronomical telescopes (Oxford University Press)

Jacquinot, P. & Roizen-Dossier, B. 1964, Progress in Optics, 3, 31

Kasdin, N. J. e. a. 2003, ApJ, 582, 1147

Kuchner, M. J. & Spergel, D. N. 2003a, in ASP Conference Series 294, Scientific Frontiers In Research In Extrasolar Planets, ed. D. Deming & S. Seager (2003)

Kuchner, M. J. & Spergel, D. N. 2003b, ApJ, 594, 617

Kuchner, M. J. & Traub, W. A. 2002, ApJ, 570, 900

Lieber, M. D. e. a. 2003, in Techniques and Instrumentation for Detection of Exoplanets. Edited by Coulter, Daniel R. Proceedings of the SPIE, Volume 5170, pp. 66-78 (2003)., 66–78

Lyot, B. 1939, MNRAS, 99, 580

Malbet, F. 1996, A&AS, 115, 161

McCarthy, D. W. e. a. 2001, PASP, 113, 353

Nisenson, P. & Papaliolios, C. 2001, ApJ, 548, L201

Roberts, L. C. & Neyman, C. R. 2002, PASP, 114, 1260

Sivaramakrishnan, A. e. a. 2001, ApJ, 552, 397

Spergel, D. N. 2001, astro-ph/0101142

This preprint was prepared with the AAS LaTeX macros v5.2.

Table 1. Table of the parameters and positioning used for the Mt. Wilson and Lab apertures. These paramters are described in relation to Equations 5 and 13.

GAPM Design	α	a	b	x_k	y_k	h
Mt. Wilson	2.7	0.23	0.33	($\pm$0.3125,$\pm$0.1625,$\pm$0.1625)	(0.1,0.2125.,0.3875)	0.5
Lab	2.7	1.	-	0	0	0.8

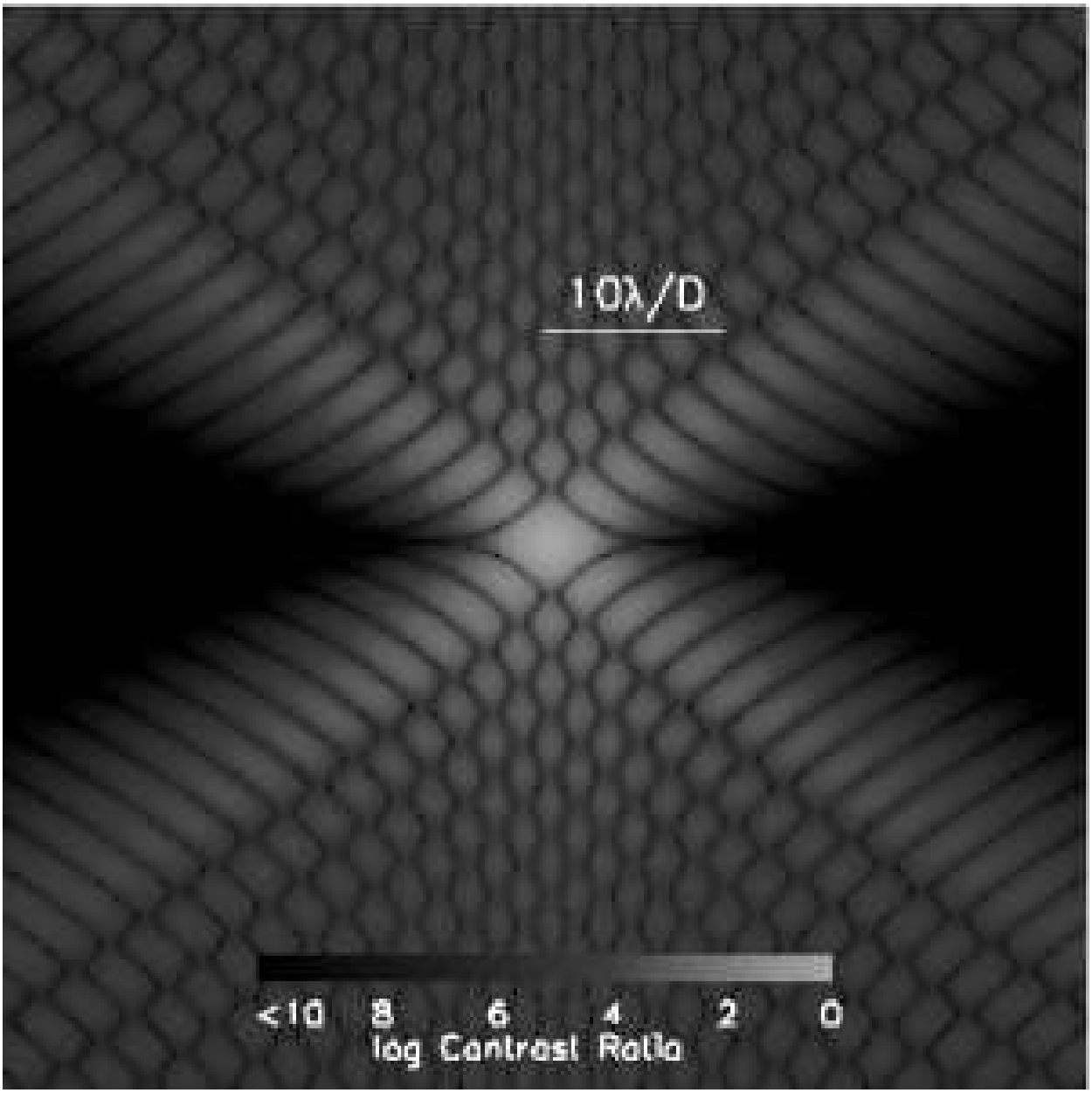

Fig. 1.— The resulting monochromatic diffraction pattern for a single aperture GAPM with $a = 1.$ and $\alpha = 2.5$. The image is logarithmically scaled.

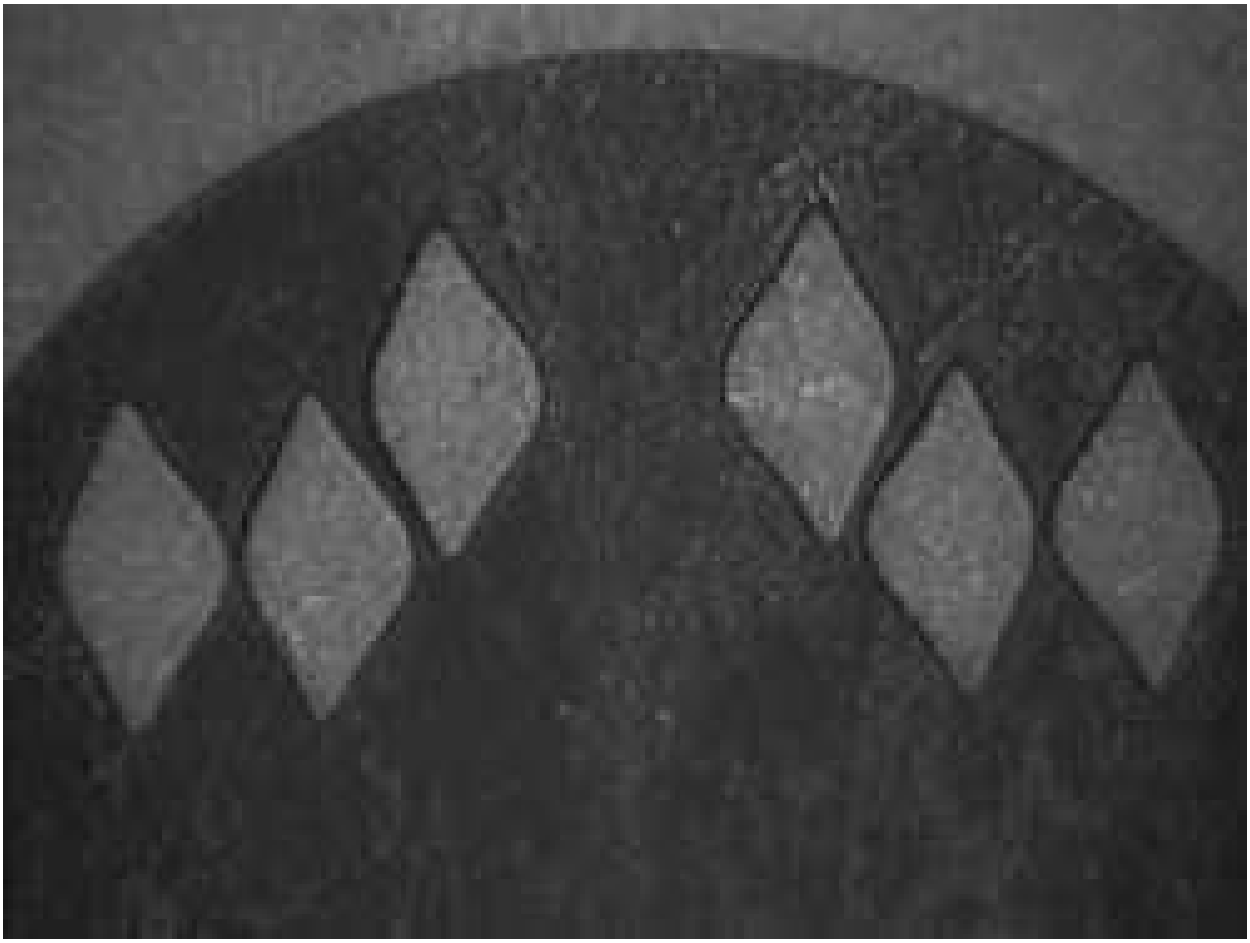

Fig. 2.— The top half of the fabricated mask used for observing on the Mt. Wilson telescope at 5x optical magnification. The twelve apertures allow ∼25% throughput, while avoiding the support structure of the telescope. This picture shows the imperfections in the fabrication process.

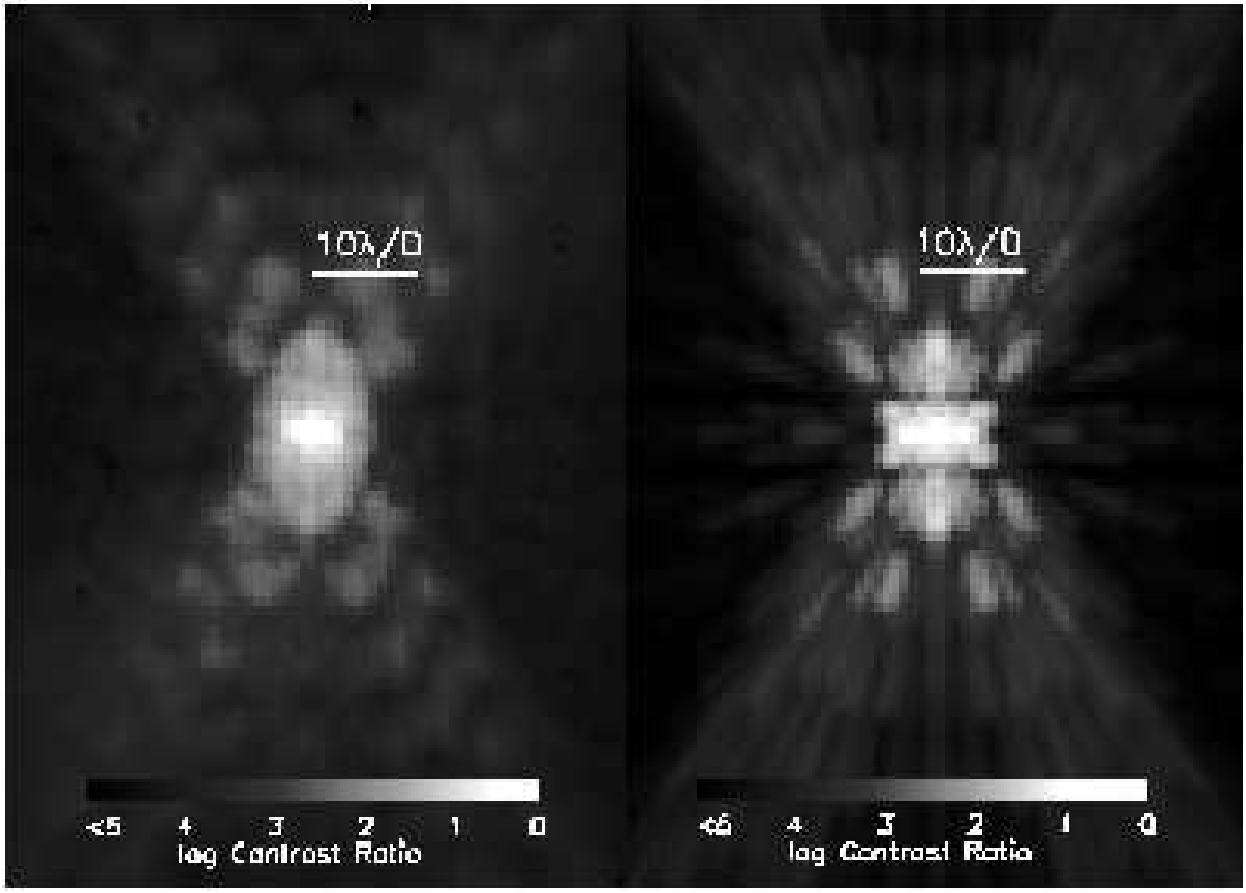

Fig. 3.— Comparison of the theoretical J band diffraction pattern (right) compared with lab results with PIRIS (left). Both are on the same logarithmic scale. The model used included the imperfect shape of the mask that was fabricated and was integrated over the transmission function of a typical J filter.

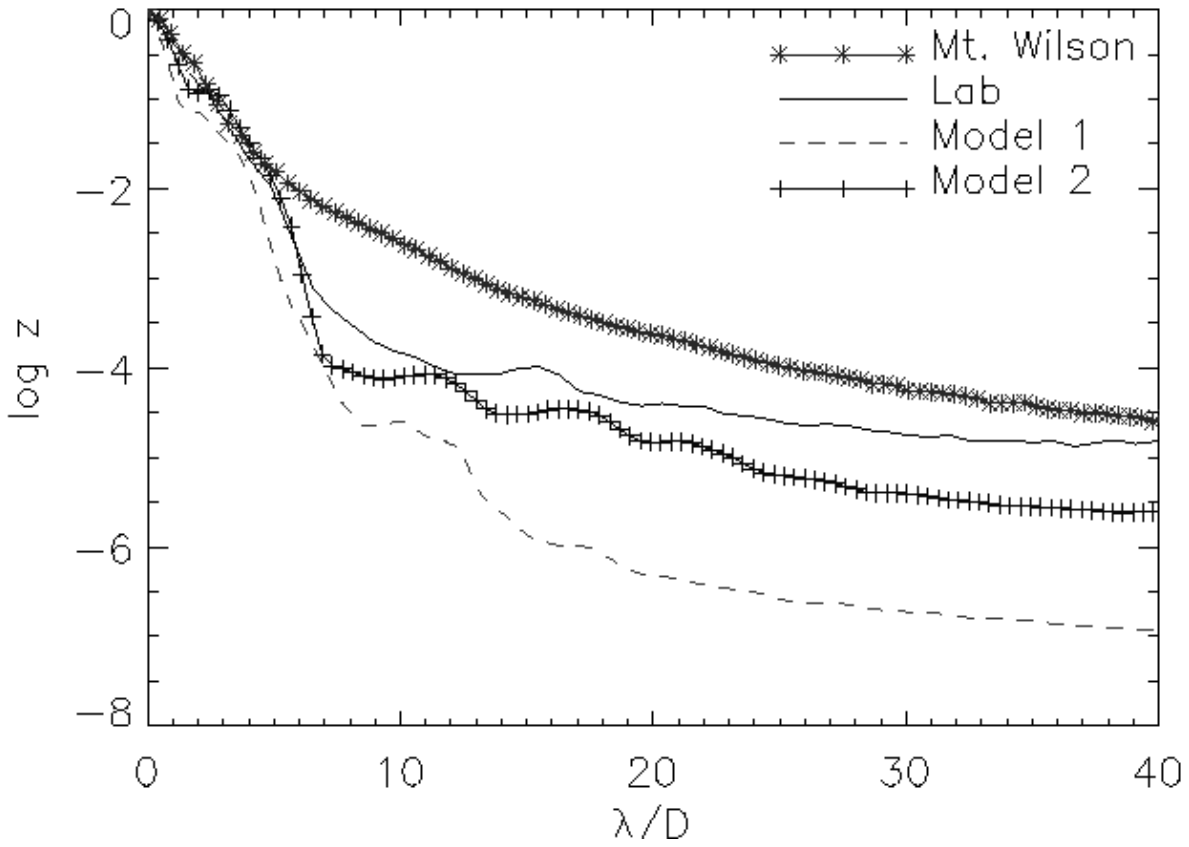

Fig. 4.— Azimuthally averaged PSF profiles for the GAPM multiaperture design tested at Mt. Wilson, along with results of a lab test in the J band and two different models. Model 1 represents a model with perfect apertures, while Model 2 is the simulated results based on the actual shape of the apertures.

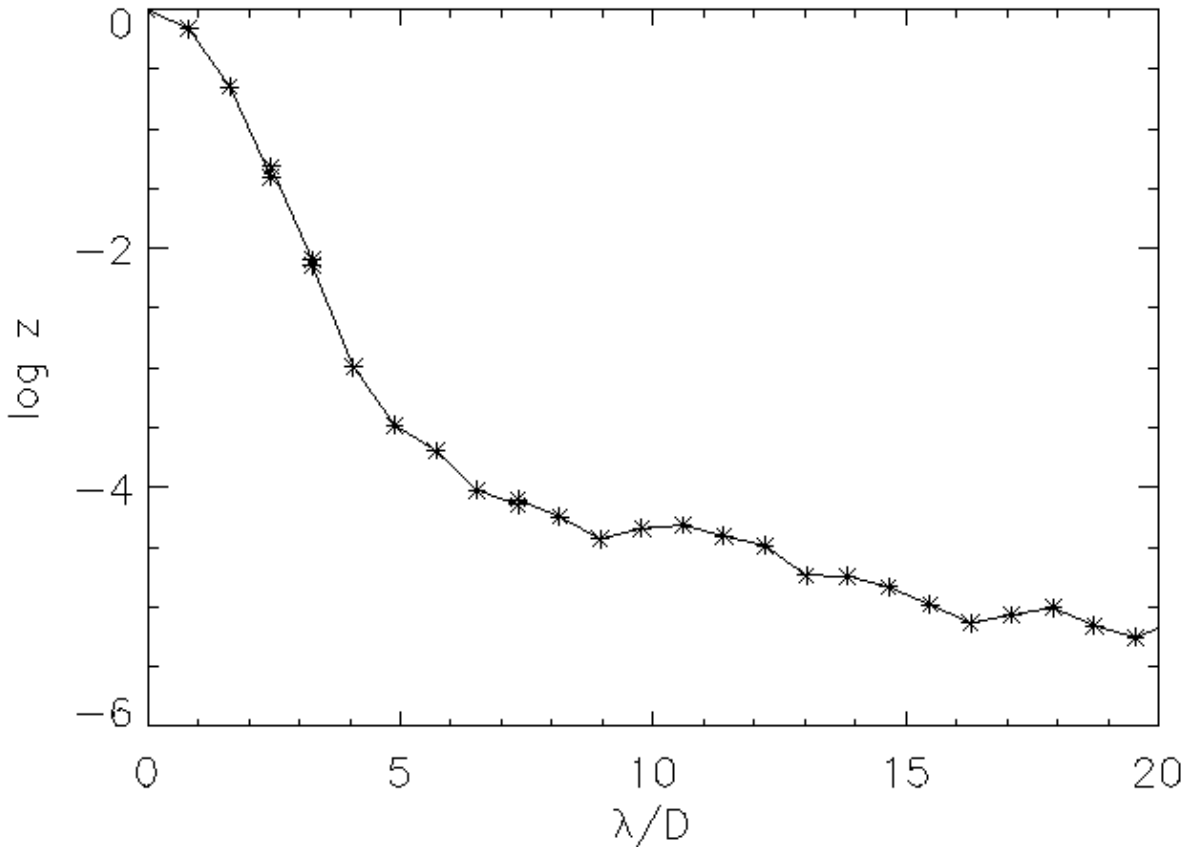

Fig. 5.— Azimuthally averaged PSF of the single aperture design in the J band. We achieved 4×10^{-5} contrast at $10\lambda/D$. Truncation of the mask during fabrication is the main degradation of contrast with what would be possible theoretically.

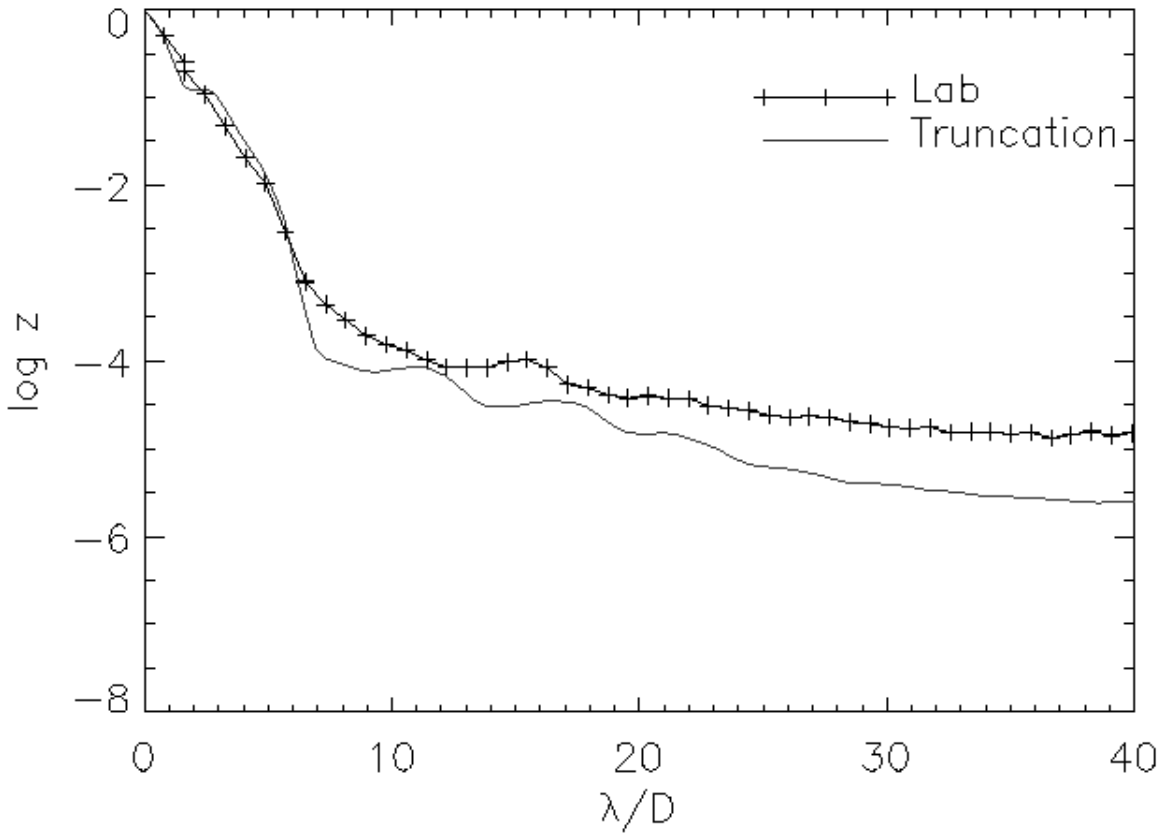

Fig. 6.— A comparison between the J band PSF and a model based on the truncation of the Gaussian contour's wings described in Equation 16. For the model we used β=13 and the parameters listed in Table 1 for the Mt. Wilson design. Both the model and the lab data were azimuthally averaged for 20° about the high contrast axis.